Turkish Journal of Electrical Engineering & Computer Sciences

http://journals.tubitak.gov.tr/elektrik/

Research Article

Turk J Elec Eng & Comp Sci
(2016) 24: 2806 – 2824

doi:10.3906/elk-1404-174

Design of compact octagonal slotted hexagonal and rectangular shaped monopole antennas for dual/UWB applications

Praveen Naidu VUMMADISETTY[1], **Raj KUMAR**[2,*]
[1]Department of Electronics and Telecommunication, Symbiosis International University, Pune, India
[2]Department of Armament Electronics, Armament Research and Development Establishment, Pashan, Pune, India

Received: 10.04.2014 • **Accepted/Published Online:** 06.12.2014 • **Final Version:** 15.04.2016

Abstract: Two CPW-fed compact printed slot antennas for UWB applications are proposed in this paper. In both antennas, the slot in the ground plane is of octagonal shape, while the patch is rectangular in one of the antennas and hexagonal in the other. Thin metallic stubs of different lengths are added to the ground plane and protrude into the slot. These stubs help to improve the impedance matching over a broader bandwidth. The antennas are very compact in size and designed on low-cost FR4 substrate. The measured impedance bandwidths ($S_{11} < -10$ dB) achieved by the rectangular and hexagonal patch antennas are from 3.1 GHz to 5.6 GHz and 3.14 GHz to 5.34 GHz, respectively. The slot antenna with hexagonal patch is further modified to have dual-band characteristics. An L-shaped stub is attached to the ground plane to achieve an additional band from 2.45 GHz to 2.52 GHz for WLAN applications. The radiation patterns of the antennas are dumb-bell shape in the E-plane and omnidirectional in the H-plane. Detailed parametric studies of the antennas have been carried out. The simulated results are found to be in good agreement with the measured results.

Key words: CPW-fed antenna, monopole antenna, ultrawideband antenna

1. Introduction

In 2002, the Federal Communications Commission (FCC) had allotted a frequency spectrum range from 3.1 GHz to 10.6 GHz for unlicensed ultrawideband (UWB) communications (https://transition.fcc.gov/Bureaus/Engineering_Technology/Orders/2002/fcc02048.pdf). After that, many researchers have paid attention to the design of compact antennas for UWB. There are two standard approaches for UWB systems, i.e. DS-CDMA (direct-sequence code division multiple access) and MB-OFDM (multiband orthogonal frequency division multiplexing). The DS-CDMA approach divides the full band into three modes of operation, i.e. a low band consisting of frequencies ranging from 3.1 GHz to 5.15 GHz, a high band consisting of frequencies ranging from 5.82 GHz to 10.6 GHz, and a multiband or mixed band consisting of frequencies ranging from 3.1 GHz to 10.6 GHz. MB-OFDM divides the full band of 3.1 GHz to 10.6 GHz into 14 subbands, each with a bandwidth of 528 MHz, and each subband is composed of 128 tones and is modulated using OFDM. The lower three subbands (3.168 GHz to 4.752 GHz) are decided as mandatory mode (Group A) in the MB-OFDM system, which can provide more than 100 Mbps data rate (IEEE Document P802.15-03/268r1, September 2003; https://www.ieee.org/). As shown in Figure 1, Group A has three channels, 3168–3696 MHz (Channel 1), 3696–4224 MHz (Channel 2), and 4224–4752 MHz (Channel 3).

*Correspondence: dr.rajkumarkumar@yahoo.com

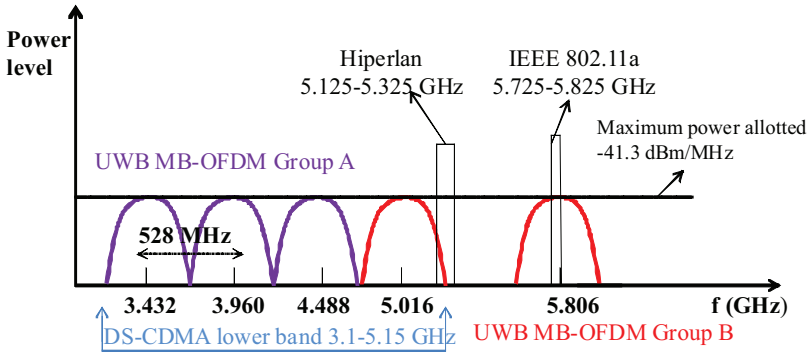

Figure 1. Frequency band of MB-OFDM and DS-CDMA.

To implement the MB-OFDM/DS-CDMA approach, UWB antennas of compact size, omnidirectional radiation patterns, and constant gain are required. Recently many researchers have reported UWB antennas [1–22] for MB-OFDM/low-band DS-CDMA systems with a frequency range of 3.1 GHz to 4.8 GHz/3.1 GHz to 5.15 GHz. In [1], a compact 20 mm × 30 mm tree shaped fractal UWB antenna was presented for MB-OFDM lower three band (3.1–4.8 GHz) applications. A 26 mm × 41.8 mm coplanar waveguide (CPW)-fed balanced wideband dipole antenna was proposed for 3-7 GHz UWB applications in [2]. A compact 30 mm × 30 mm filter combined UWB antenna for 3.1 GHz to 5.2 GHz DS-CDMA/MB-OFDM applications was proposed in [3]. A CPW-fed, pentagonal cut fractal antenna (31 mm × 32 mm) was presented in [4] for 4.69 GHz to 15 GHz DS-CDMA higher band applications. A compact 30 mm × 20 mm monopole antenna with two symmetrical strips for 3.1–4.8 GHz frequency band operation was proposed in [5]. In [6] a 50 mm × 67 mm diamond shaped fractal antenna was designed using the CPW-fed technique for UWB applications with frequency range from 2.0 GHz to 6.2 GHz. A U-shaped open stub CPW-fed antenna was proposed in [7] for dual frequency applications. The proposed design has overall dimensions of 35 mm × 30 mm and works for 2.4 GHz WLAN and 3.0 GHz to 6.0 GHz UWB applications. Similarly, various monopole antennas were reported in [8–11] for 3.0 GHz to 5.15 GHz frequency operation but these antennas have the drawback of larger size in comparison with our proposed designs. Various dual-band antennas were also presented in [12–15]. In [12], a 25 mm × 25 mm microstrip-fed antenna was proposed for dual frequency band applications. By using a meander in the ground plane, lower frequency at 2.44 GHz was generated, and by using an L-shaped radiator higher resonance frequency at 5.8 GHz was achieved. Similarly, for achieving dual-band operation a bow-tie shaped slot in [13], U-shaped slot in [14], and rectangular slot in [15] were used in the antenna design. A 120 mm × 100 mm slot antenna was proposed in [16] by using the microstrip-feeding technique. For achieving an UWB from 3.1 GHz to 10.6 GHz a square ring slot was introduced in the structure. Various slot antennas with different dimensions were reported in [17–22] for WLAN/UWB applications. A comparison study of all the UWB and dual-band antennas mentioned in references [1–21] in terms of overall size and bandwidth achieved is given in Table 1. Though some of the referenced antennas cover the entire UWB band, those antennas have the drawback of large dimensions. As a result, it is very difficult to integrate the antenna with other RF and MIMO circuits.

In this paper, two compact CPW-fed octagonal slot antennas with hexagonal and rectangular shaped patches are designed. These antennas have bandwidths of 2.5 GHz (3.10–5.6 GHz) and 2.20 GHz (3.14–5.34 GHz), respectively. In addition, an UWB and dual-band antennas are also presented in Sections 7 and 8. These designs offer an extended bandwidth up to 9.2 GHz (3.1 GHz to 12.3 GHz) in the case of UWB antenna design and an additional band centered at 2.5 GHz in the case of dual-band antenna design, respectively. All the

above designed antennas have more compact size (20 mm × 20 mm) compared to the reference antennas. The antennas are designed, simulated, and optimized using CST Microwave Studio 3D-electromagnetic software and validated experimentally. The proposed antennas can be used for DS-CDMA/MB-OFDM (Group A) UWB systems.

Table 1. Comparison of the proposed antenna with reference antennas.

Serial. no. No	Reference	Antenna type	Size (mm × mm)	Operating band
1.	Ref [1]	UWB	30 × 20	3.1–4.8 GHz
2.	Ref [2]	UWB	26 × 41.8	3.1–4.8 GHz
3.	Ref [3]	UWB	30 × 30	3.1–5.2 GHz
4.	Ref [4]	UWB	31 × 32	4.69–15 GHz
5.	Ref [5]	UWB	30 × 20	3.1–4.8 GHz
6.	Ref [6]	UWB	50 × 67	2.0–6.2 GHz
7.	Ref [7]	Dual-band	35 × 30	2.45 GHz & 3–6 GHz
8.	Ref [8]	UWB	40 × 100	3.1–5.15 GHz
9.	Ref [9]	UWB	24 × 25	3.1–5.1 GHz
10.	Ref [10]	UWB	20 × 30	3.1–4.8 GHz
11.	Ref [11]	UWB	24 × 25	3.1–5.1 GHz
12.	Ref [12]	Dual band	25 × 25	2.38–2.51 GHz & 4.79–5.98 GHz
13.	Ref [13]	Dual-band	60 × 45	2.26–2.57 GHz & 4.81–6.56 GHz
14.	Ref [14]	Dual-band	40 × 40	2.4–2.484 GHz & 5.15–5.825 GHz
15.	Ref [15]	Dual-band	75 × 75	2.4 GHz & 5 GHz
16.	Ref [16]	Single-band	120 × 100	3.1–10.6 GHz
17.	Ref [17]	Single-band	45 × 21.5	3.0–10 GHz
18.	Ref [18]	Single-band	85 × 85	2.8–14 GHz
19.	Ref [19]	Single-band	66.1 × 44	3.1–12 GHz
20.	Ref [20]	Single-band	90 × 90	4.71–6.14 GHz
21.	Ref [21]	Single-band	100 × 100	3.1–10.6 GHz
22.	Proposed antenna	Dual band	20 × 20	2.5 GHz & 3.0–6.0 GHz

2. Antenna structure

The geometries of the proposed antennas are shown in Figure 2. The antennas are designed on FR-4 substrate having thickness of 1.58 mm and permittivity of 4.3. The ground plane is printed on one side of the substrate. An octagonal slot is etched on the ground plane for both antennas. The radiating element is a hexagonal patch for one of the antennas and a two-stepped rectangular patch for the other. The hexagonal patch's height (denoted by 'g10' in Figure 2a) gives higher cut-off frequency near 5.15 GHz while the hexagonal patch's width 'g9' is optimized to get the best return loss characteristic. Another parameter in the design that has to be optimized to ensure good return loss performance is the vertical separation between the patch and the ground plane. This parameter is denoted by 'g5' and its optimal value is found to be equal to 3 mm. For the rectangular patch antenna, the patch's height, 'g13' (Figure 2b), gives the higher cut-off frequency near 5 GHz, while the patch's width, 'g8', is optimized to get the best return loss characteristic. Three vertical stubs are added to the octagonal shaped ground section for better impedance matching. The vertical separation between the patch and the lower ground plane is denoted by 'b10' and its optimal value is found to be equal to 3.5 mm. The dimensions of all the parameters of the two antennas are listed in Tables 2 and 3, respectively.

Figure 3 shows the different stages in the design of the proposed hexagonal patch antenna and the corresponding reflection coefficients are shown in Figure 4. The initial design (Antenna #1a) as seen in Figure

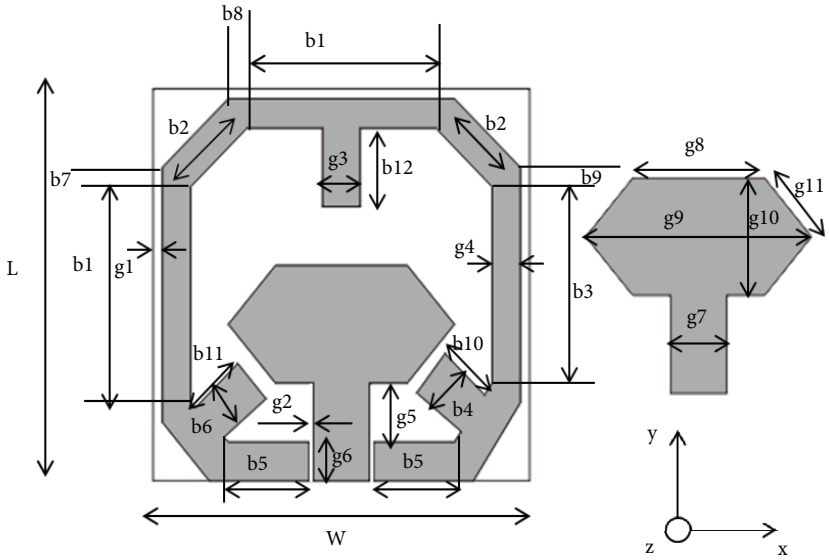

Figure 2. a)Proposed hexagonal patch antenna.

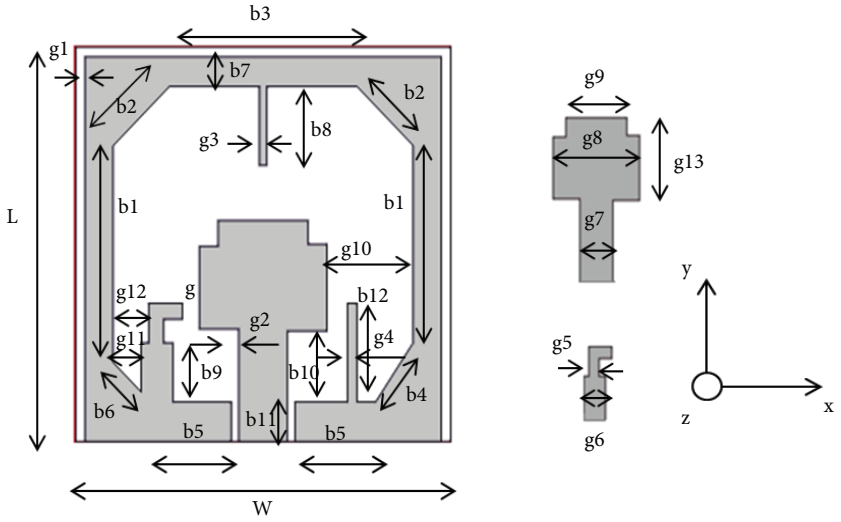

Figure 2. b) Proposed rectangular patch antenna.

Table 2. Optimal parameters of the proposed hexagonal patch antenna.

Parameter	W	L	b1	b2	b3	b4	b5	b6	b7	b8
Value (mm)	20	20	11	4.2	10	2.5	4.3	2.5	1	0.5
Parameter	b9	b10	b11	b12	g1	g2	g3	g4	g5	g6
Value (mm)	1	3	3.1	4	0.4	0.2	2	1.5	3	2
Parameter	g7	g8	g9	g10	g11					
Value (mm)	3	7	12	6	3.9					

3 consists of a hexagonal shaped patch surrounded by octagonal shaped slot etched on the ground plane and excited by a 50 Ω CPW feed line. To enhance the impedance bandwidth, the initial design is modified and the modified versions are named Antenna #2a, Antenna #3a, and proposed antenna. It can be seen in Figure 4 that there is an improvement in the impedance bandwidth along with enhanced impedance matching with successive modifications in the design.

Table 3. Optimal parameters of the proposed rectangular patch antenna.

Parameter	W	L	b1	b2	b3	b4	b5	b6	b7	b8
Value (mm)	20	20	11	3.6	12	2.8	4.3	2.8	1.5	4
Parameter	b9	b10	b11	b12	g1	g2	g3	g4	g5	g6
Value (mm)	3	3.7	2	5	0.5	0.4	0.4	0.5	0.8	1.7
Parameter	g7	g8	g9	g10	g11	g13	g12	g		
Value (mm)	2.6	6.8	4.8	4.6	1.5	5.5	1.8	1.0		

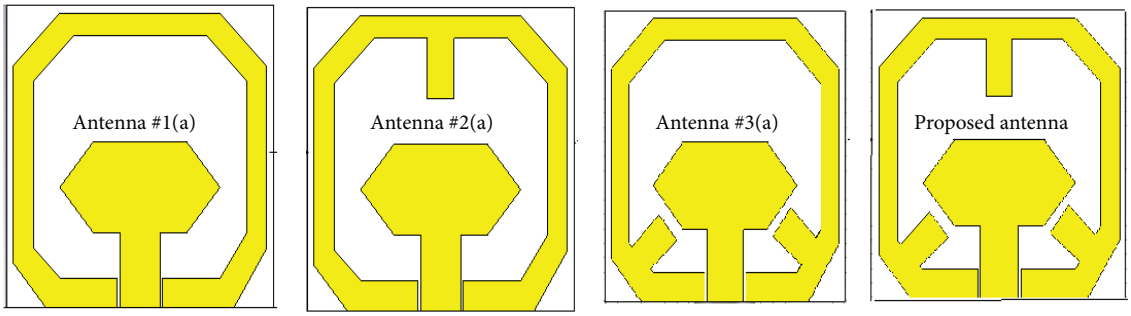

Figure 3. Different stages of the proposed hexagonal patch antenna.

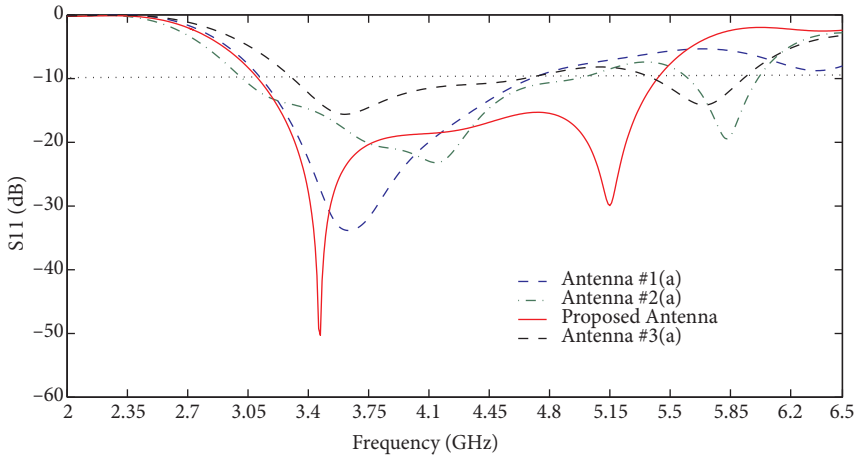

Figure 4. Simulated S_{11} for different stages of hexagonal patch antenna.

The initial designs of the rectangular patch antenna along with the modified versions are shown in Figure 5. The simulated reflection coefficients are shown in Figure 6. The slot used is similar to that of the hexagonal patch antenna. However, the tuning stubs are shaped differently. Again it can be seen in Figure 6 that there is an improvement in the impedance bandwidth with successive addition of rectangular shaped stubs in the design.

3. Measured and simulated results

The proposed two antennas (hexagonal patch and rectangular patch) are designed and fabricated with optimized dimensions. Figures 7 and 8 show the fabricated prototypes of the hexagonal and rectangular patch antennas along with their measured and simulated reflection coefficients. The measurements were performed using a Rohde & Schwarz Vector Network Analyzer (R&S ZVA-40). The measured impedance bandwidth of the

octagonal slotted rectangular patch antenna is 2.5 GHz from 3.10 GHz to 5.6 GHz and that of the hexagonal patch antenna is 2.20 GHz from 3.14 GHz to 5.34 GHz. It can be seen in the figures that the measured and simulated reflection coefficients are in good agreement. The slight difference between the measured and simulated results is due to fabrication constraints, uncertainties in the dielectric constant and substrate thickness, soldering effects, and the quality of the SMA connector used.

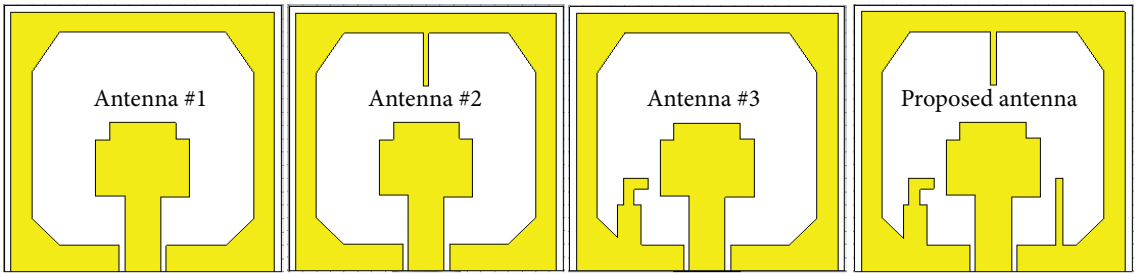

Figure 5. Different stages of the proposed rectangular patch antenna.

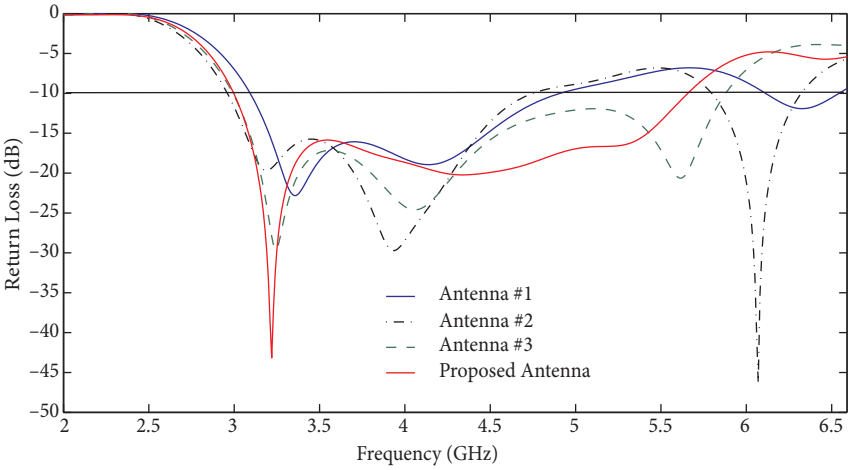

Figure 6. Simulated S_{11} for different stages of the proposed rectangular patch antenna.

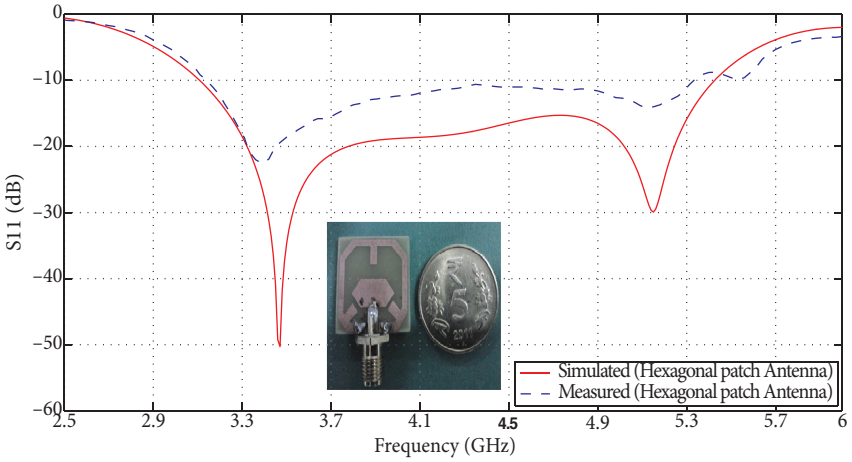

Figure 7. Photograph of the proposed hexagonal patch antenna with the corresponding simulated and measured return loss.

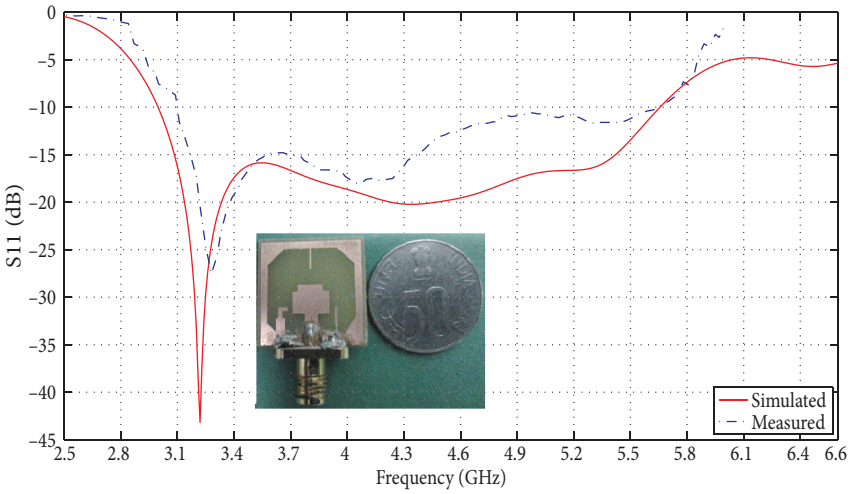

Figure 8. Photograph of the proposed rectangular patch antenna with the corresponding simulated and measured return loss.

4. Theoretical analysis

The contributing factor for the first resonance (f_{H1} = 3.46 GHz and f_{R1} = 3.25 GHz) seen in the simulated S_{11} curves (Figures 7 and 8) of the proposed hexagonal and rectangular patch antennas is due to the octagonal slot perimeter. The resonance frequencies for these two antennas are approximately obtained from Eqs. (1) and (2). The second resonances (near 5.15 GHz and 5.05 GHz) are due to the patch height and also affected by the coupling between the lower edge of the patch and the upper edge of the ground plane. As given in [23], the second resonance frequencies are obtained from Eqs. (3) and (4).

$$f_{H1} = \frac{C}{l_1\sqrt{\varepsilon_{r,eff}}} \tag{1}$$

$$f_{R1} = \frac{C}{L_1\sqrt{\varepsilon_{r,eff}}} \tag{2}$$

$$f_2 = \frac{C}{4l_2\sqrt{\varepsilon_{r,eff}}} \tag{3}$$

$$f_3 = \frac{C}{4l_3\sqrt{\varepsilon_{r,eff}}} \tag{4}$$

$$l_1 + L_1 = 2b_1 + 2b_2 + b_3 + b_4 + 2b_5 + b_6 \tag{5}$$

$$l_2 = g_5 + g_{10} \tag{6}$$

$$l_3 = b_{10} + g_{13} \tag{7}$$

$$L_2{+}H_7{+}H_{10}{+}H_{11}{+}H_{12}{+}H_{13}{+}H_{14}{+}H_{15}{+}H_{16}\varepsilon_{r,eff} = \frac{\varepsilon_r + 1}{2} \tag{8}$$

Here, c stands for the velocity of light in free space; l_1 and L_1 are the slot perimeters of the hexagonal and rectangular patch antennas, respectively; and l_2 and l_3 are the effective monopole heights of hexagonal and rectangular patch antennas, respectively, while $\varepsilon_{r,eff}$ is the effective relative permittivity to be calculated using Eq. (8). For calculating the effective relative permittivity, it is assumed that for a CPW-fed monopole, half of the established field lies in the air while the remaining half is distributed in the substrate. The first and second resonance frequencies are calculated using Eqs. (1)–(8). Table 4 shows the comparison between calculated and simulated resonance frequencies.

Table 4. Comparison between calculated and simulated resonances.

Resonance frequency	Calculated value	Simulated value
f_{H1} (hexagonal patch, first resonance)	3.39 GHz	3.46 GHz
f_{R1} (rectangular patch, first resonance)	3.30 GHz	3.25 GHz
f_2 (hexagonal patch, second resonance)	5.08 GHz	5.17 GHz
f_3 (rectangular patch, second resonance)	4.98 GHz	5.05 GHz

The return loss or resonance frequency characteristics of the hexagonal and rectangular shaped patch antennas can also be explained by observing the current distributions on the proposed antennas. The surface current distributions for the hexagonal patch antenna at 3.5 GHz and 5.25 GHz are given in Figures 9a and 9b, while for the rectangular patch at 3.25 GHz and 5.25 GHz they are given in Figures 9c and 9d. In Figure 9, the red color indicates maximum current density while blue indicates minimum current density. It can be seen that at lower frequencies maximum current is distributed on the octagonal slot and there is much less current on the patch. Similarly, at the high frequencies maximum current is distributed on the patch and there is much less current on the octagonal slot. Thus, the current distributions justify the conclusions drawn previously wherein, for both antennas, the lower resonances were attributed to the slot and the higher resonances were attributed to the patch.

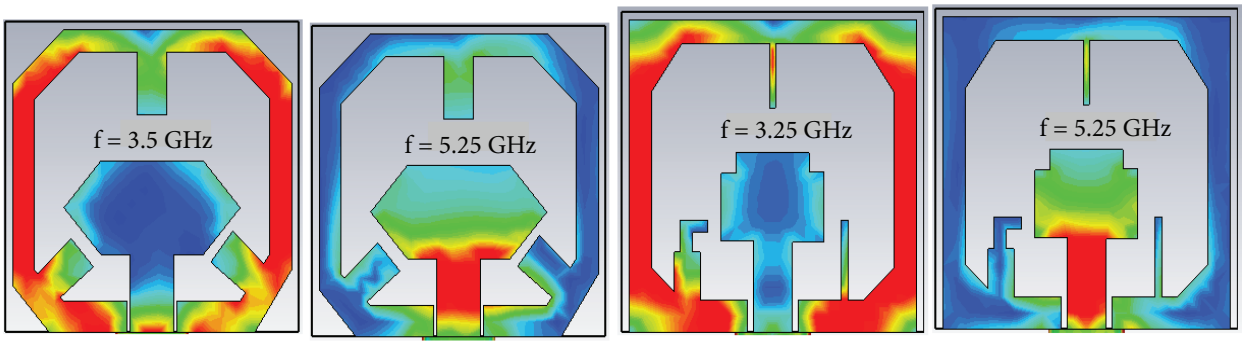

Figure 9. Surface current distribution for hexagonal patch (a, b) and rectangular patch (c, d) antennas.

5. Parametric study

5.1. Hexagonal shaped patch antenna

5.1.1. Effect of varying the separation between patch and lower ground

The separation between the patch and the ground plays a crucial role in obtaining wider impedance bandwidth. Figure 10 shows the variation in return loss by varying the separation between the patch and the ground. It can

be seen that a smaller separation gives better impedance matching at higher frequencies, whereas a larger value improves the impedance matching at the lower frequencies. Hence, the separation 'g5' needs to be optimized and the optimum value is found to be 3.0 mm. At this optimum value, the maximum coupling of electromagnetic energy between the patch and the ground is achieved in wider bandwidth.

5.1.2. Effect of varying the gap between feed line and ground

The gap between the feed line and the ground plane 'g2' is an important factor that decides the feed line impedance. The effect of varying the gap between the feed line and the ground (by fixing feed width 'g7' = 3 mm) on the return loss is shown in Figure 11. It is seen that an increase in the gap between the feed line and ground plane increases the return loss due to impedance mismatch. For a small gap of 'g2' = 0.2 mm, the imaginary part of the feed impedance approaches zero while the real part approaches 50 Ω to get optimized broad impedance matching.

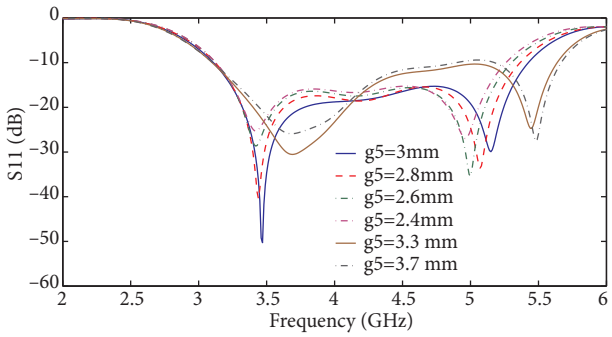

Figure 10. Effect of the patch-ground separation 'g5' on return loss.

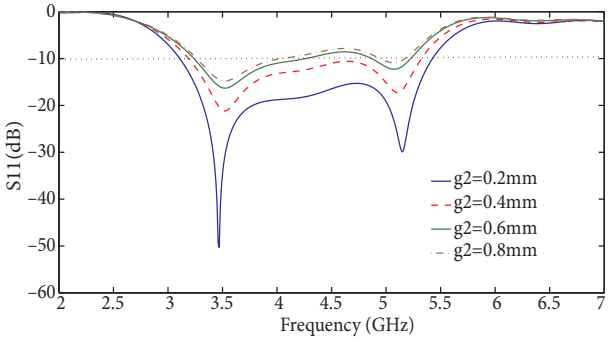

Figure 11. Effect of the separation gap 'g2' between feed line and ground on return loss.

5.1.3. Effect of varying the patch height

The effect of varying the patch height 'g10' on the return loss is shown in Figure 12. The second resonance is attributed to the patch and it is seen that with an increase in the patch height, the second resonance shifts towards the lower side. The first resonance is also affected due to the varying coupling between the upper part of the patch and one of the tuning stubs attached to the ground plane. The increase in the coupling diverts more current towards the tuning stub and shortens the path of the loop current, thus increasing the resonant frequency. As far as the impedance matching is considered, an optimal value is found at 'g10' = 6 mm.

5.1.4. Effect of varying the height of tuning stub 'b12'

The effect of varying the height of the rectangular tuning stub of the hexagonal patch antenna is shown in Figure 13. Here, the stub height varies from 3 mm to 5.5 mm with a step of 0.5 mm by keeping stub width fixed at 'g3' = 2 mm. It is observed from Figure 13 that the first resonance is affected slightly while the second resonance is strongly affected. With an increase in the stub length, the second resonance shifts towards the lower side. The overall impedance matching improves up to a certain value for the stub length and then deteriorates. The optimized value for 'b12' is found to be 4 mm.

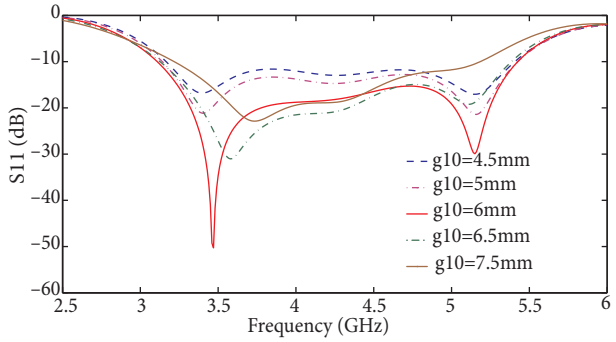

Figure 12. Effect of the patch height 'g10' on return loss.

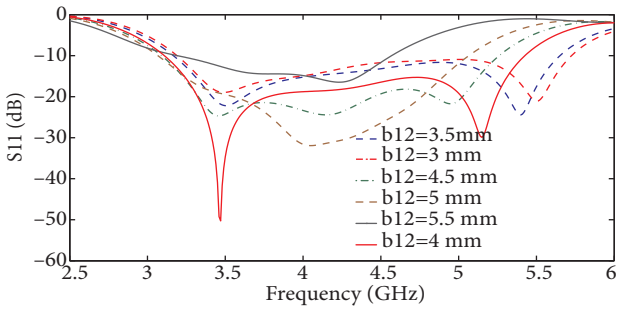

Figure 13. Effect of height 'b12' on the performance of the proposed antenna.

5.2. Rectangular shaped patch antenna

5.2.1. Effect of varying the separation between ground and patch

The variations in the reflection coefficient magnitude with the ground-patch separation 'b10' are shown in Figure 14. It can be observed from the figure that the operating band can be divided into three subbands that respond differently to a change in the separation. While the impedance matching at central frequencies seems to improve with a decrease in the separation, the impedance matching at the other two ends improves with a decrease in the separation. Again, an optimal value has to be found, which is obtained as 2.0 mm for broader bandwidth.

5.2.2. Effect of varying the rectangular tuning stub height

The effect of varying the dimensions of the rectangular tuning stub of the proposed antenna is presented. The octagonal slot and rectangular patch dimensions remain unchanged in the study. The variations in the reflection coefficient characteristics with variations in the height 'b8' of the narrow rectangular stub are illustrated in Figure 15. It can be observed from the figure that as the height of 'b8' increases the lower and higher resonances shift towards the lower side. However, the shift in the higher resonance is more than the shift in the lower resonance. Hence, there is a change in the bandwidth. The optimal value for 'b8' is achieved as 4 mm.

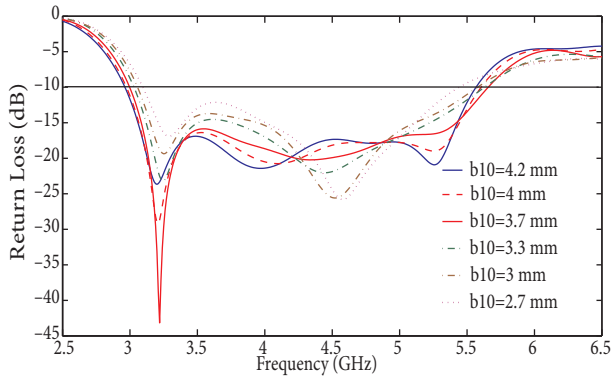

Figure 14. Effect of the separation 'b10' on the performance of the proposed antenna.

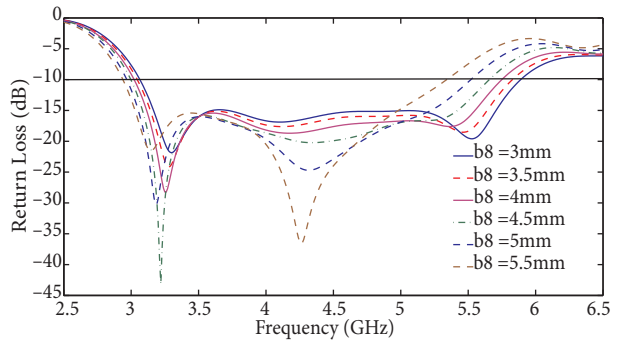

Figure 15. Effect of height 'b8' on the performance of the proposed antenna.

6. Radiation patterns and peak gain

The radiation patterns of the two slot antennas are simulated using CST Microwave Studio and measured in an in-house anechoic chamber using an antenna measurement system. A standard double ridged horn antenna is used as a reference antenna. The simulated and measured radiation patterns of the octagonal slotted hexagonal shaped patch antenna are shown in Figures 16a–16c for different frequencies (3.5 GHz, 4.3 GHz, and 5.1 GHz). Similarly, the radiation patterns in the E-plane and H-plane of the octagonal slotted rectangular shaped patch antenna are shown in Figures 16d–16f for different frequencies (3.6 GHz, 4.4 GHz, and 5.0 GHz). The nature of H-plane radiation patterns is omnidirectional while the E-plane radiation patterns are bidirectional (dumb-bell shaped). For both cases, the simulated and measured results are found to be in close agreement with a little difference due to measurement and alignment errors.

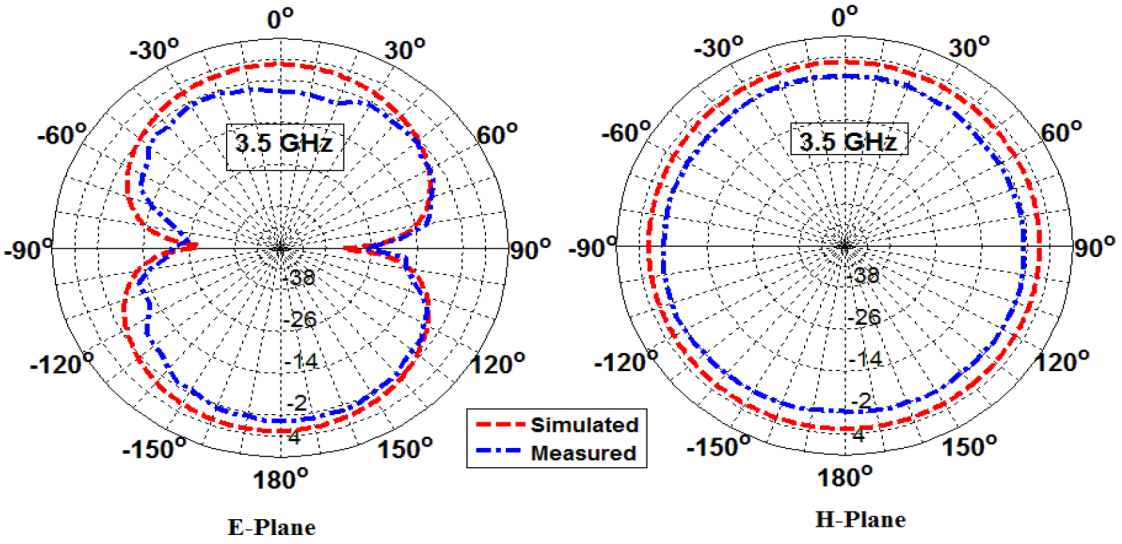

Figure 16. a) Radiation patterns of the hexagonal patch antenna at 3.5 GHz.

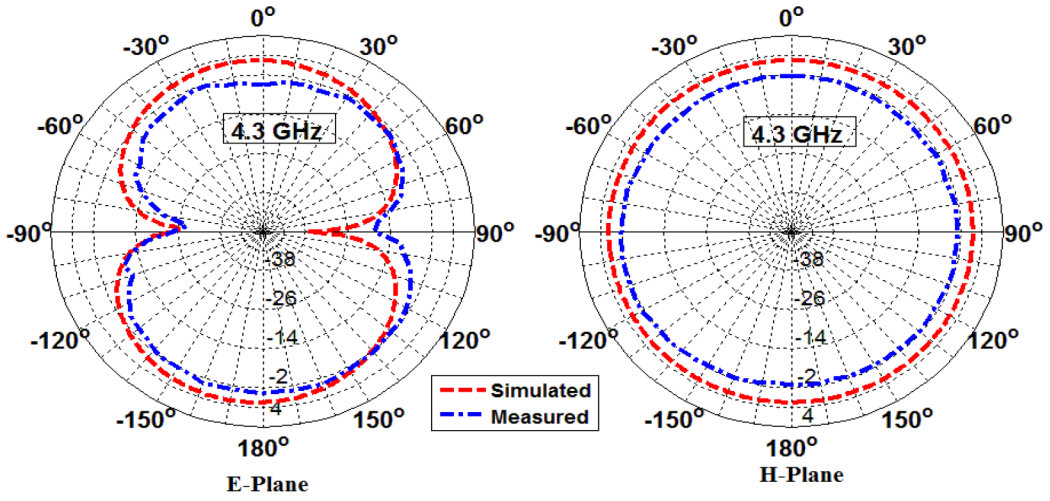

Figure 16. b) Radiation patterns of the hexagonal patch antenna at 4.3 GHz.

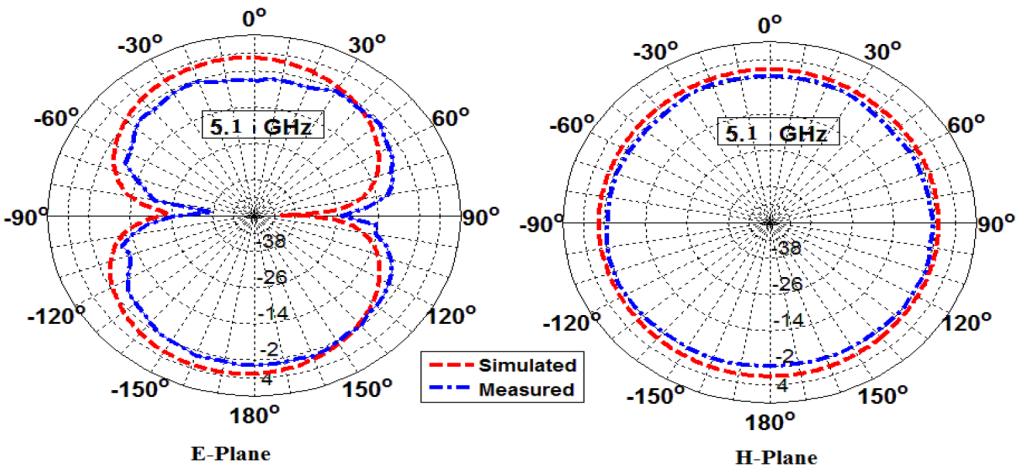

Figure 16. c) Radiation patterns of the hexagonal patch antenna at 5.1 GHz.

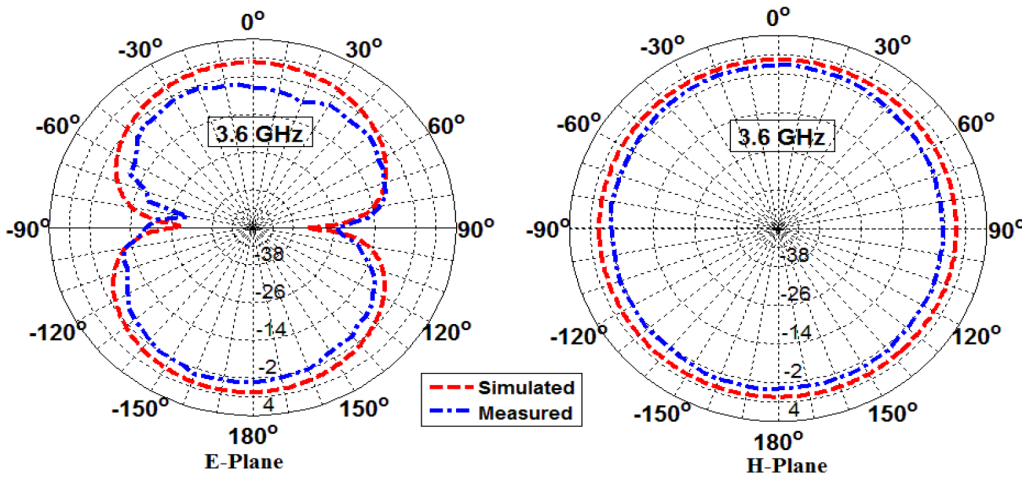

Figure 16. d) Radiation patterns of the rectangular patch antenna at 3.6 GHz.

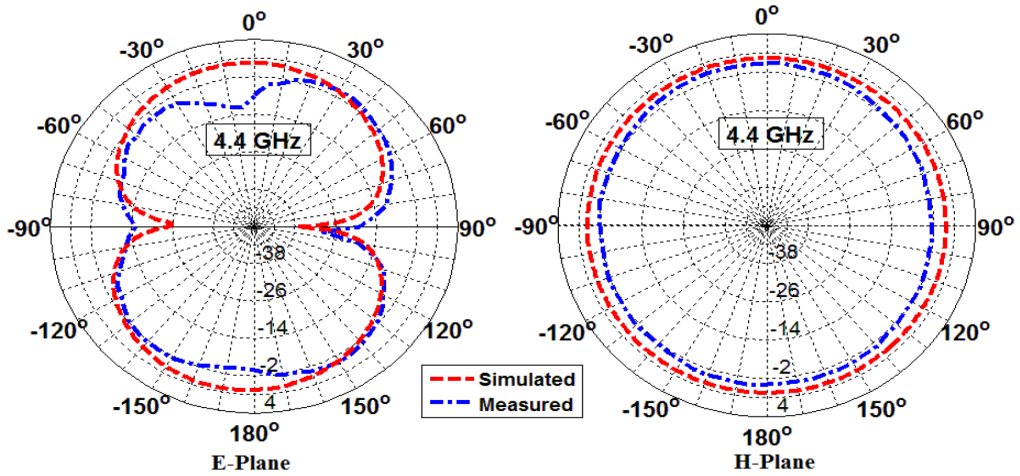

Figure 16. e) Radiation patterns of the rectangular patch antenna at 4.4 GHz.

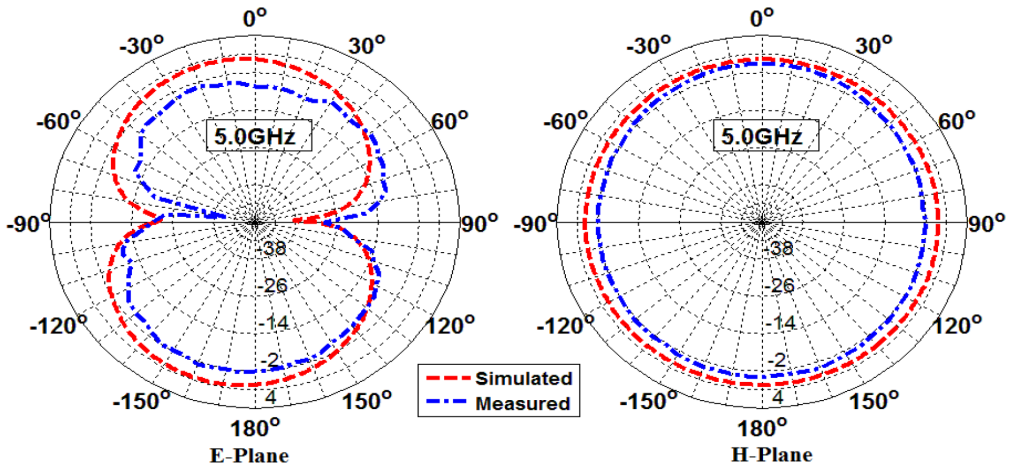

Figure 16f. Radiation patterns of the rectangular patch antenna at 5.0 GHz.

7. Modified hexagonal patch antenna for dual-band

In this section, a modified version of the hexagonal patch antenna to generate dual-band is shown. For this antenna the structure and dimensions are considered as nearly same as the antenna designed in Section 2. The proposed antenna geometry and its corresponding optimized parameter values are given in Figure 17 and Table 5, respectively. By adding an L-shaped stub to the ground plane, a new band is generated at 2.5 GHz. The length of the stub is 16.5 mm, which nearly corresponds to $\lambda/4$ at the resonance frequency (2.5 GHz). A photograph of the fabricated antenna and comparison of measured and simulated return loss are shown in Figure 18. To illustrate how the length of the stub controls the added resonance, a parametric variation in the horizontal part of the stub 'b13' and its effect on the return loss is shown in Figure 19. As the stub length is increased, the added resonance shifts towards the lower side.

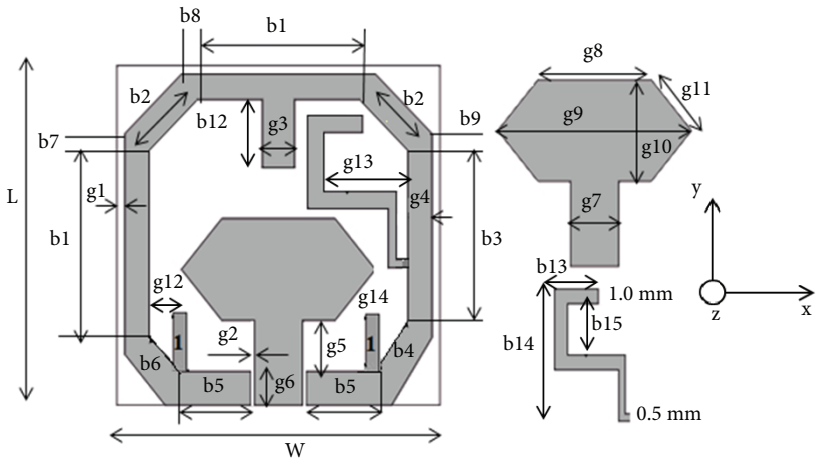

Figure 17. Proposed hexagonal patch antenna with L-shape stub for extra resonance.

The simulated peak gains across the operating bands for all the proposed antennas are shown in Figure 20. As can be seen, stable gains across desired bands have been achieved. The simulated peak gains remains between 1 and 4 dBi in the useful bands.

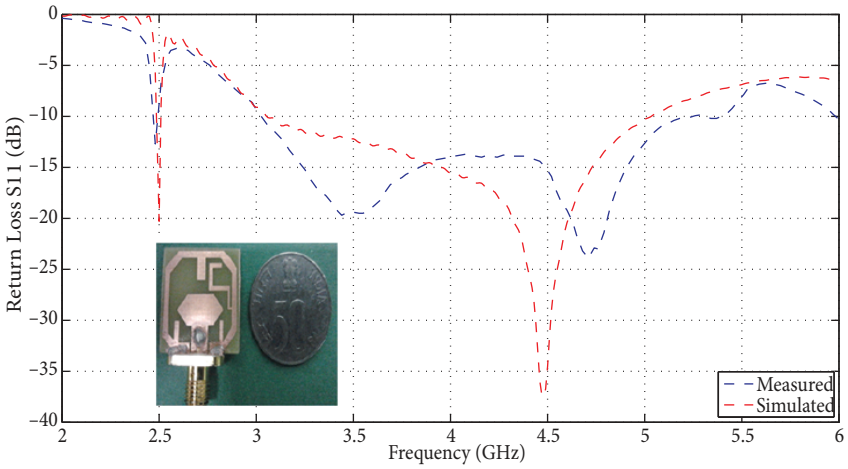

Figure 18. Photograph of the fabricated dual band antenna, measured and simulated return loss.

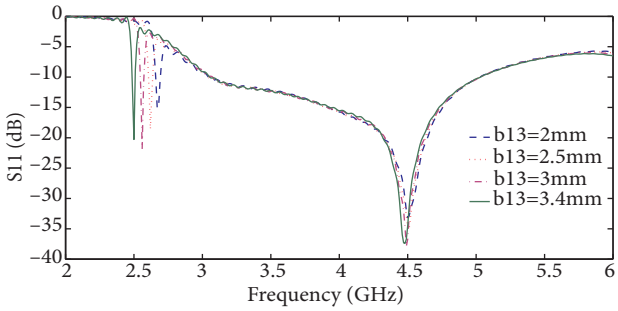

Figure 19. Effect of varying stub length on return loss.

Table 5. Optimal parameters of the proposed hexagonal patch dual-band antenna.

Parameter	L	W	b1	b2	b3	b4	b5	b6	b7
Value (mm)	20	20	11	4.2	10	2.5	4.3	2.5	1
Parameter	b8	b9	b10	b11	b12	b13	b14	b15	g1
Value (mm)	0.5	1	3	3.1	4	3.4	9	3.5	0.4
Parameter	g2	g3	g4	g5	g6	g7	g8	g9	g10
Value (mm)	0.2	2	1.5	3	2	3	7	12	6
Parameter	g11	g12	g13	g14					
Value (mm)	3.9	2.1	5	4					

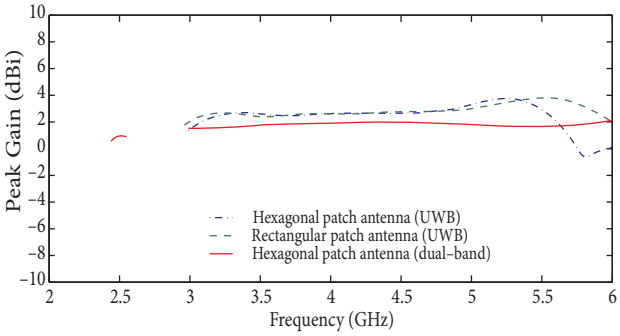

Figure 20. Comparison of simulated peak gains of all the antennas.

8. UWB antenna design

In order to operate the antenna over the entire UWB range (3.1 GHz to 10.6 GHz), the antenna proposed in Section 2 has been modified and a new design is proposed, given in Figure 21. This proposed antenna consists of a simple rectangular patch, an L-shaped stub, and an asymmetric staircase shaped ground structure. The overall dimensions (20 mm $\times$ 20 mm) of the antenna are kept the same as in other proposed designs in Section 2. The optimized dimensions of the antenna are given in Table 6. The simulated reflection coefficient (S11) for the proposed antenna is shown in Figure 22. From the figure, it can be seen that the –10 dB impedance bandwidth is around 9.2 GHz, starting from 3.1 GHz to 12.3 GHz.

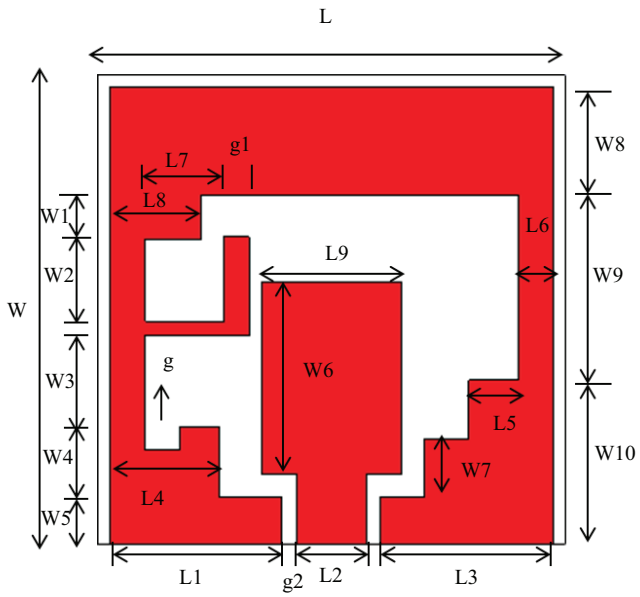

Figure 21. Structure of the proposed UWB antenna.

Table 6. Final parameter values of the proposed antenna.

Parameter	L	W	L1	L2	L3	L4	L5	L6	L7
Value (mm)	20	20	7.3	2.9	7.4	4.6	2.1	2	3.4
Parameter	L8	L9	W1	W2	W3	W4	W5	W6	W7
Value (mm)	3.9	6	2	3.5	3.9	3	2	8.2	2.5
Parameter	W8	W9	W10	g	g1	g2			
Value (mm)	4.6	7.9	7	1	1.1	0.7			

Figure 23a shows the evolutionary stages of the UWB antenna and its corresponding return loss characteristics are given in Figure 23b. The initial design is a simple rectangular slot containing a rectangular patch. The bandwidth achieved with this design is 4.5 GHz, from 2.9 GHz to 7.4 GHz. In stage 2 (Figure 23a), by changing the simple rectangular ground plane profile to an asymmetric slot, bandwidth is extended to 6 GHz from 3.0 GHz to 9 GHz. Next, in stage 3, a staircase profile is introduced to the ground plane; as a result, good return loss improvement is achieved at higher frequencies. Finally, by adding an L-shaped stub to the ground plane nearer to the patch, a good return loss (below –10 dB) in the 5 GHz to 6 GHz band and also good impedance matching in the entire UWB are achieved. Figure 24 shows the simulated surface current distribution of the proposed UWB slot antenna. The current distribution is shown at four frequencies. It can

be seen in the figure that for the proposed UWB antenna, at 3.5 GHz maximum current is distributed on the slot and much less or zero current is distributed on the patch and on the L-shaped stub. This clearly indicates that the first resonant frequency is due to the slot perimeter and expression in terms of the slot perimeter 'Z1' given in Eq. (9). From Figure 24 it is seen that at 4.8 GHz frequency, the surface current is more on the patch and slot. This indicates that the resonance at 4.8 GHz frequency is because of the monopole height 'Z2'. The expression for the second resonance frequency can be approximated by equating the height of the rectangular patch to λeff/4 and it is given in Eq. (10). Due to the L-shaped stub and asymmetric staircase shape, the ground plane and fundamental harmonics of the first two resonant frequencies of the overall bandwidth of the proposed antenna have been improved. This can be understood by observing the current distribution at 6.5 GHz and 9 GHz in Figure 24.

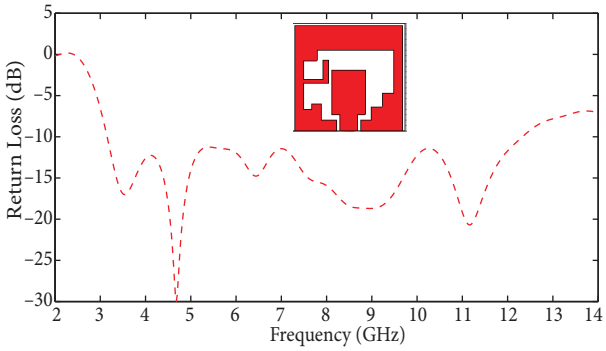

Figure 22. Simulated return loss of the proposed UWB antenna.

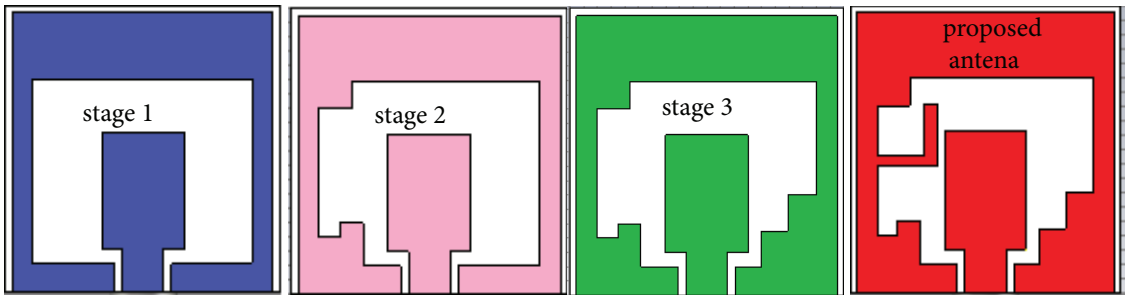

Figure 23. a) Evaluation stages of the proposed UWB antenna.

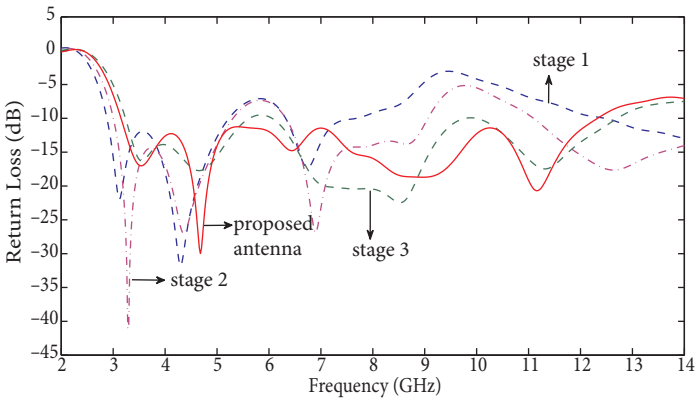

Figure 23. b) Simulated return loss against frequency for different stages of the UWB antenna.

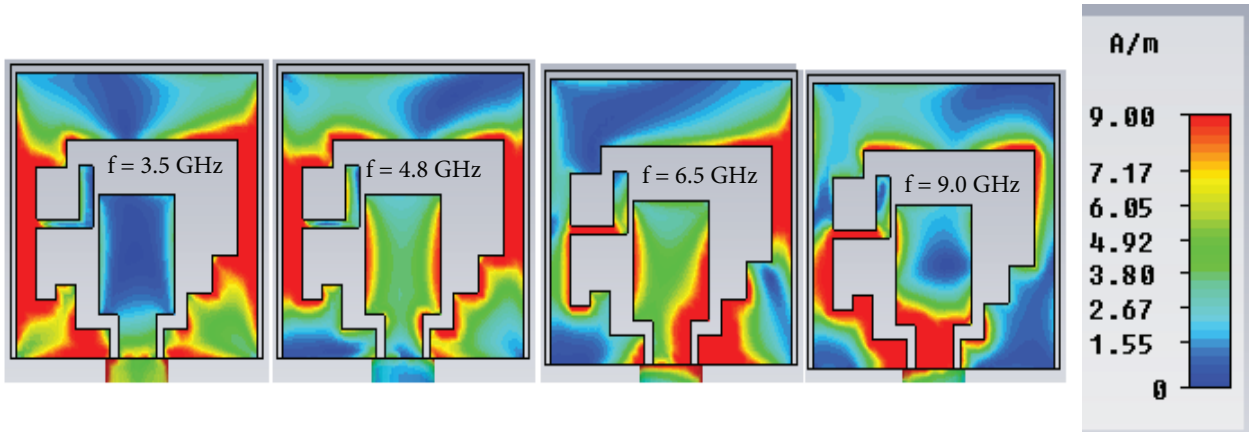

Figure 24. Current distribution at different resonance frequencies of UWB antenna.

$$f_{UWB1}=\frac{C}{Z_1\sqrt{\varepsilon_{r,eff}}} \tag{9}$$

$$f_{UWB2}=\frac{C}{4Z_2\sqrt{\varepsilon_{r,eff}}} \tag{10}$$

$$Z_1=(L1-L4)+W4+(L4-L6)+W2+W3+(L8-L6)+W1+(L-L8)+W9+2(L5+W7) \tag{11}$$

$$Z_2=(W6+W7/2) \tag{12}$$

$$L_2+H_7+H_{10}+H_{11}+H_{12}+H_{13}+H_{14}+H_{15}+H_{16}\varepsilon_{r,eff}=\frac{\varepsilon_r+1}{2} \tag{13}$$

Here, c stands for the velocity of light in free space, while $\varepsilon_{r,eff}$ is the effective relative permittivity to be calculated using Eq. (13). For calculating the effective relative permittivity, it is assumed that for a CPW-fed monopole, half of the established field lies in the air while the remaining half is distributed in the substrate.

The simulated peak gains of the proposed UWB antenna as a function of frequency are shown in Figure 25. It can be seen in the figure that peak gain remains between 1.5 dBi and 3 dBi in the UWB region (3.1 GHz to 10.6 GHz). At higher frequencies the peak gain increases with frequency due to the increased effective area of the antenna at shorter wavelengths. The constant peak gain with good impedance bandwidth makes the proposed antenna suitable for UWB communication applications.

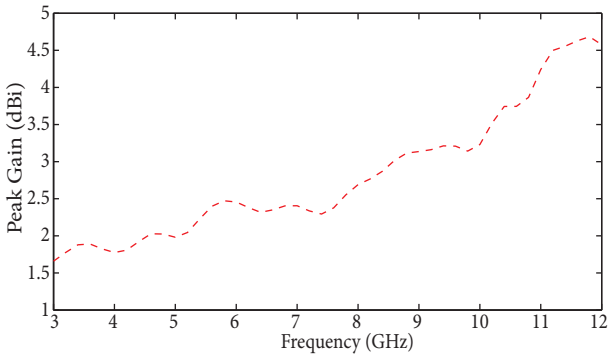

Figure 25. Simulated peak gains of the proposed antennas.

9. Conclusions

Two CPW-fed UWB slot antennas have been designed and experimentally validated. The slot is octagonal in shape and the radiating elements are rectangular and hexagonal shaped patches. The measured impedance bandwidth obtained is 2.5 GHz at the center frequency of 4.35 GHz for the rectangular patch antenna and 2.2 GHz at the center frequency of 4.24 GHz for the hexagonal patch antenna. By introducing an additional L-shaped stub in the ground plane, a dual-band response is obtained in case of the hexagonal patch antenna. The radiation patterns of both antennas are omnidirectional in the H-plane and bidirectional in the E-plane. The peak gain is in an acceptable range. These antennas are simple to design and easily integrated with MIC/MMIC devices. These antennas have potential applications for WLAN and DS-CDMA/MB-OFDM (Group A) UWB systems.

Acknowledgment

The first author is a doctoral student at Symbiosis International University (Deemed University), Pune, India, and doing research under the guidance of Dr. Raj Kumar and also acknowledges his support for availing the Microwave and Millimeter wave Antenna Laboratory Facilities at DIAT (DU).

References

[1] Park JK, An HS, Lee JN. Design of the tree-shaped UWB antenna using fractal concept. Microw Opt Techn Let 2008; 50: 144-150.

[2] Chan KCL, Huang Y. A novel CPS-fed balanced wideband dipole for ultra-wideband applications. In: First European Conference on Antennas and Propagation; 6–10 November 2006; Nice, France. pp. 1-4.

[3] Lee JN, Park JK, Choi IIH. A compact filter-combined ultra-wide band antenna for UWB applications. Microw Opt Techn Let 2008; 50: 2839-2845.

[4] Kumar R, Chaubey PN. On the design of CPW-fed pentagonal-cut UWB fractal antenna. Int J Microw Opt Techn 2011; 6: 249-254.

[5] Song HW, Park JK, Yoo JH. A novel ultra-wideband monopole antenna with two symmetrical strips. Microw Opt Techn Let 2008; 50: 2845-2848.

[6] Kumar R, Malathi P. On the design of CPW-fed diamond shape fractal antenna for UWB applications. Int J Electron 2011; 98: 1157-1168.

[7] Lee JN, Kim JH, Park JK, Kim JS. Design of dual-band antenna with U-shaped open stub for WLAN/UWB applications. Microw Opt Techn Let 2009; 51: 284-289.

[8] Lee JN, Park JK. Compact UWB chip antenna design using the coupling concept. Prog Electromagn Res 2009; 90: 341-351.

[9] Yazdanboost KY, Kohno R. Ultra wideband L-loop antenna. In: IEEE International Conference on Ultra-Wideband; 5–8 September 2005; Zurich, Switzerland. pp. 201-205.

[10] Song HW, An HS, Lee JN, Park JK, Kim JS. Design of the tree-shaped UWB antenna using fractal concept. In: Korea-Japan Microwave Conference; 15–16 November 2007; Okinawa, Japan. pp. 73-76.

[11] Yazandoost KY, Kohno R. UWB antenna for wireless body area network. In: Asia Pacific Microwave Conference; 12–15 December 2006; Yokohoma, Japan. pp. 1647-1652.

[12] Sun XL, Cheung SW, Yuk TI. A compact monopole antenna for WLAN applications. Microw Opt Techn Let 2014; 56: 469-475.

[13] Tsai LC. A triple-band bow-tie-shaped CPW-fed slot antenna for WLAN applications. Prog Electromagn Res C 2014; 47: 167-171.

[14] Flores RL, Jardon HA, Tirado AM, Acevo RH. Reduced microstrip slot multiband antenna with AU-shaped resonator for WLAN applications. Microw Opt Techn Let 2012; 54: 2684-2689.

[15] Wu JW, Hsiao HM, Lu JH, Chang SH. Dual broadband design of rectangular slot antenna for 2.4 and 5 GHz wireless communication. Electron Lett 2004; 40: 1461-1463.

[16] Sadat S, Fardis M, Geran FG, Dadashzadeh GR. A compact microstrip square-ring slot antenna for UWB applications. Prog Electromagn Res 2007; 67: 173-179.

[17] Azenui NC, Yang HYD. A printed crescent patch antenna for ultrawideband applications. IEEE Antenn Wirel Pr 2007; 6: 113-116.

[18] Dastranj A, Biguesh M. Broadband coplanar waveguide-fed wide-slot antenna. Prog Electromagn Res C 2010; 15: 89-101.

[19] Ma TG, Tseng CH. An ultrawideband coplanar waveguide-fed tapered ring slot antenna. IEEE T Antenn Propag 2006; 54: 1105-1110.

[20] Mitra D, Das D, Bhadra Chaudhuri SR. Bandwidth enhancement of microstrip line and CPW-fed asymmetrical slot antennas. Prog Electromagn Res Lett 2012; 32: 69-79.

[21] Dawood SJ, Salari MA, Ghoochani OH. Cross-slot antenna with U-shaped tuning stub for ultra-wideband applications. International Journal of Antennas and Propagation 2008; 2008: 262981.

[22] Kumar R, Naidu PV, Kamble V. Design of asymmetric slot antenna with meandered narrow rectangular slit for dual band applications. Prog Electromagn Res B 2014; 60: 111-123.

[23] Kushwaha N, Kumar R, Ram Krishna RVS. Design of CPW-fed asymmetric slot UWB antenna for wireless application. Journal of Electronics (China) 2014; 31: 341-347.